**Technical Paper**

ISSN 1997-1400 Int. J. Pavement Res. Technol. 8(2):94-102


# Effects of Mineral Admixtures on Microstructure-linked Strength Properties of Macro-synthetic Fiber Reinforced Concrete

Rui He[1+,2,3], Juan-lan Zhou[4], Ping-ming Huang[4], Bo-wen Guan[1,2], and Yan-ping Sheng[1,2]

**Abstract:** This study investigates the effects of fly ash and silica fume on the mechanical properties and microstructure characteristics of interfacial transition zone (ITZ) between macro-synthetic fiber and the bulk matrix of the fiber reinforced concrete. The experimental results show that the concrete is able to withstand significant post-cracking loads and undergo remarkable deflections under flexural loads due to the bridging effect of macro-synthetic fiber. The mechanical properties of concrete incorporating fly ash plus silica fume are much better than those prepared with no mineral admixtures or mono addition. The work of adhesion is an integrated index to evaluate the bonding behaviors between fiber and matrix, which exhibits a trend similar to that noted in the flexural toughness. The compound addition of fly ash and silica fume presents the most distinct improvement effects on microstructure of ITZ and the bonding behaviors between fiber and matrix. The amount of hydrated calcium silicate (C-S-H) gel and compaction of ITZ play key roles in the fiber - matrix interfacial bond and the mechanical properties of concrete.

**DOI**: 10.6135/ijprt.org.tw/2015.8(2).94
***Key words**: Fiber reinforced concrete; Interfacial transition zone; Macro-synthetic fiber; Microstructure; Mineral admixtures.*

## Introduction

Reinforcements with fiber have proven to be an effective and economical way to eliminate the brittle failures of concrete structures under dynamic loads [1-3]. Randomly distributed fibers were employed to enhance the resistance to both crack initiation and propagation [3, 4]. Moreover, the positive effects of fibers on ductility, energy absorption and toughness were also investigated. The mechanical properties of fiber reinforced concrete (FRC) are mainly dependent on the performance of fiber, matrix, and fiber-matrix interface. Due to the wall effect and bleeding, the matrix at the vicinity of fiber surface shows higher porosity compared to the bulk matrix, forming an interfacial transition zone (ITZ) between the fiber and the bulk matrix. Therefore, a sound knowledge of the fiber-matrix interaction is of key importance for predictions and design of the optimum mechanical properties of composite materials [5, 6].

Because of its important role in cementitious composite materials, the performance of ITZ between fiber and matrix has been studied extensively. Caggiano *et al.* [5] proposed a unified formulation for simulating the overall bond behavior of fibers embedded in cementitious matrices on the basis of assuming a model between interface bond stresses and the corresponding relative displacements. Pakravan *et al.* [7] evaluated the adhesion of nylon66, PP and acrylic fibers to a cement matrix both by a theoretical and by an experimental approach, and found that the fracture energy due to the interfacial interactions is several orders of magnitude smaller than the polymeric fiber losses function. Tosun-Felekoglu *et al.* [8] investigated the effects of fiber type and matrix modification on the multiple cracking performance of cementitious composite. It was indicated that the toughening improvement mechanisms of PP and PVA fibers are extremely different and matrix modifications significantly change the multiple cracking performance. Sun *et al.* [9] reported that the addition of silica fume can eliminate the poor characteristics of interface layer between steel fiber and cement matrix, leading to the great improvement of fatigue life of steel fiber reinforced concrete. Hu *et al.* [10] chose three types of polymer emulsions to modify the properties of steel fiber reinforced cementitious composites and found that the interfacial layer between steel fiber and matrix is strengthened by the chemical reaction between polymers and cement matrix. Sadrmomtazi *et al.* [11] noted that the compressive and flexural strength of PP fiber reinforced composites can be effectively improved by incorporating nano-$SiO_2$ as the reduction of internal porosity and higher friction in the fiber/matrix transition zone caused by nano-$SiO_2$.

In most practical situations, synthetic fibers could not provide adequate interfacial bond strength with the surrounding matrix. A considerable amount of work has been done to evaluate or improve the bonding performance of fiber-matrix interface. Macro-synthetic fiber, an embossed tape fiber with the same width and thickness dimension as steel fiber, has been produced recently with the promise of creating an alternative to steel fibers in structural applications [12, 13]. To the best of our knowledge, the research about the adhesion between the macro-synthetic fiber and the matrix is limited. It seems that the physical and chemical effects of mineral admixtures can be useful in the reduction of the wall effect between the synthetic macro fiber and matrix, and enhance the bonding strength due to their finer grain effect and high activity. Moreover,

[1] School of Materials Science and Engineering, Chang'an University, Xi'an 710061, China.
[2] Engineering Research Center of Ministry of Education for Transportation Materials, Chang'an University, Xi'an 710061, China.
[3] Guangxi Key Laboratory Cultivation Base for Road Structure and Material, Guangxi Transportation Research Institute, Nanning 530007, China.
[4] School of Highway, Chang'an University, Xi'an 710064, China.
[+] Corresponding Author: E-mail heruia@163.com
Note: Submitted June 23, 2014; Revised January 13, 2015; Accepted January 14, 2015.

incorporating industrial by-product, for example, fly ash or silica fume, could also create a positive environmental effect for the reduction of carbon dioxide emission.

Accordingly, the present study focuses on the effect of mineral admixtures on the microstructure associated mechanical properties of macro-synthetic fiber reinforced concrete, namely the flexural and compressive strength and the bonding behaviors between fiber and matrix. It is essential to investigate both the mechanical properties and the microstructure from the same specimen in order to have a thorough understanding of the effects taking place. Thus, the fiber/matrix bonding performances were analyzed and related to the fracture mechanism that occurred in the composites. The microstructures of ITZ between macro-synthetic fiber and matrix were then analyzed via scanning electron microscope (SEM) and micro-hardness tester.

## Experimental Program

### Materials

The binding materials used in this research included: ordinary Portland cement (type P.O. 42.5, China), low- calcium fly ash (class I, China), and silica fume (class SF93, China). The chemical compositions of cement, fly ash and silica fume are stated in Table 1, and the micro-appearances of the mineral admixtures are shown in Fig. 1. Both fly ash and silica fume exhibit good microsphere morphology. Macro-synthetic fibers, which were manufactured from a proprietary blend of polypropylene resins, with a density of 0.95 g/cm$^3$, a length of 28 mm, a diameter of 800 μm and elongation capacity of 15% were chosen for the production of FRCs (Fig. 2). The elastic modulus and tensile strength of these fibers were 7 GPa and 530 MPa, respectively. Crushed limestone with a maximum size of 20 mm and relative density of 2.65 was chosen for coarse aggregate, while river sand with fineness modulus of 2.25 was used as fine aggregate. A polycarboxylate based superplasticizer was adopted to adjust the workability of the fresh mixtures.

**Table 1.** Chemical Compositions of Cement, Fly Ash and Silica Fume.

| Constituents (%) | Cement | Fly Ash | Silica Fume |
|---|---|---|---|
| CaO | 63.98 | 5.86 | 0.46 |
| $SiO_2$ | 21.68 | 46.83 | 95.13 |
| $Al_2O_3$ | 5.34 | 30.79 | 0.61 |
| $Fe_2O_3$ | 3.47 | 10.23 | 0.33 |
| $SO_3$ | 2.37 | 1.03 | 0.94 |
| MgO | 1.17 | 1.95 | 0.71 |
| $K_2O$ | 0.56 | 2.04 | 0.92 |
| $Na_2O$ | 0.45 | 0.81 | 0.73 |

### Methods

1.5 vol.% macro-synthetic fibers were incorporated into matrices with different dosages of mineral admixtures. The mix proportions of all the matrices are stated in Table 2. All numbers in Table 2 are mass ratios to binder mass. The mineral admixtures were added to the mixtures with the replacement of cement by weight. The fresh

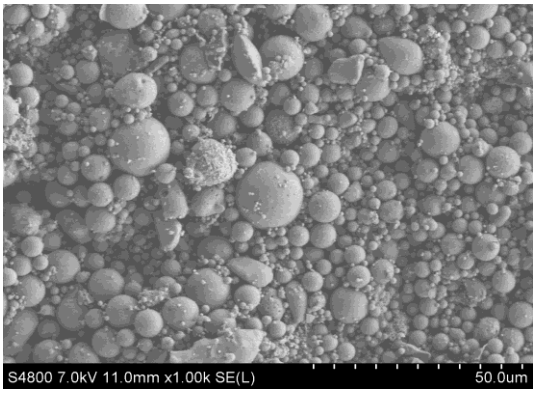


(a) fly ash

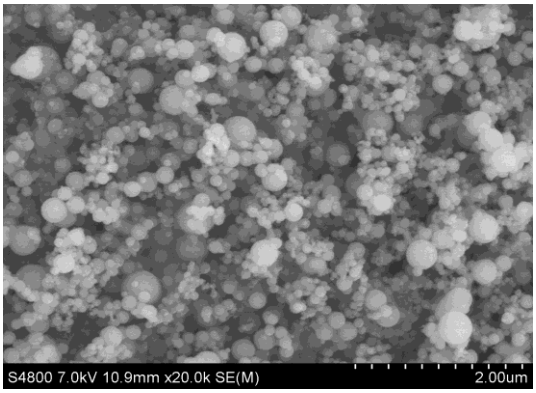


(b) silica fume

**Fig. 1** Micro-appearances of Admixtures.


**Fig. 2.** Macro-synthetic Fiber Used for Concrete Reinforcement (unit: cm).

**Table 2.** Mix Proportion of the Matrices

| Mix Code | Cement | Water | Fly Ash | Silica Fume | Sand | Coarse Aggregate | Superplasticizer |
|---|---|---|---|---|---|---|---|
| M0 | 1.00 | 0.32 | 0 | 0 | 2.05 | 2.26 | 0.01 |
| MF1 | 0.90 | 0.32 | 0.10 | 0 | 2.05 | 2.26 | 0.01 |
| MF2 | 0.80 | 0.32 | 0.20 | 0 | 2.05 | 2.26 | 0.01 |
| MS1 | 0.95 | 0.32 | 0 | 0.05 | 2.05 | 2.26 | 0.01 |
| MS2 | 0.90 | 0.32 | 0 | 0.10 | 2.05 | 2.26 | 0.01 |
| MC1 | 0.85 | 0.32 | 0.10 | 0.05 | 2.05 | 2.26 | 0.01 |
| MC2 | 0.75 | 0.32 | 0.20 | 0.05 | 2.05 | 2.26 | 0.01 |

mixtures were cast into 100 × 100 × 400 mm prism moulds immediately after the mixing. After 28 days of curing at (20±2) ℃ and 95% RH, mechanical tests were carried out with three specimens tested for each case. Four-point bending tests were performed with load and mid-span deflection measured by the computer [14]. The portions of prisms broken in bending tests were employed for compressive test according to Chinese Standard JTG E30-2005.

For investigation of bonding characteristics of single fibers, the pullout tests were carried out in a MTS Criterion40 testing machine at a crosshead rate of 0.02 mm/s. Fig. 3 shows the schematic description of the test set-up. Three replicate tests were performed for each type of composite. The load and deformation values were acquired by a PC-based data acquisition system. The matrix composition used here is the same as that of FRCs, shown in Table 2, except for the removal of coarse aggregates. Initially, a piece of foam plastic was used to fix the fiber and adjust the required embedded length (12 mm). Then, cement mortar was introduced to the vacant space in the mold. After demolding at 24 h, specimens were subjected to a curing room for 28 days at the same condition of the concrete specimens mentioned above.

In order to identify the effect of mineral admixtures on the microstructure of the ITZ between fiber and matrix, a cube of 10 × 10 × 10 mm was subsequently cut from the middle of the prism using a diamond saw and polished for micro-observation and micro-hardness tests. The samples were polished with 600 # paper then 1500 # paper to obtain an adequately smooth surface with minimal damage. An S-4800 field emission gun scanning electron microscope (Hitachi) and a MH-5 micro-hardness apparatus (Shanghai Jvjing) were employed in the microstructure analysis. During the micro-hardness test, instance from test point center to interface was a little bigger than half of trace diagonal. Three parallel points to interface were tested and used to calculate the average value of hardness.

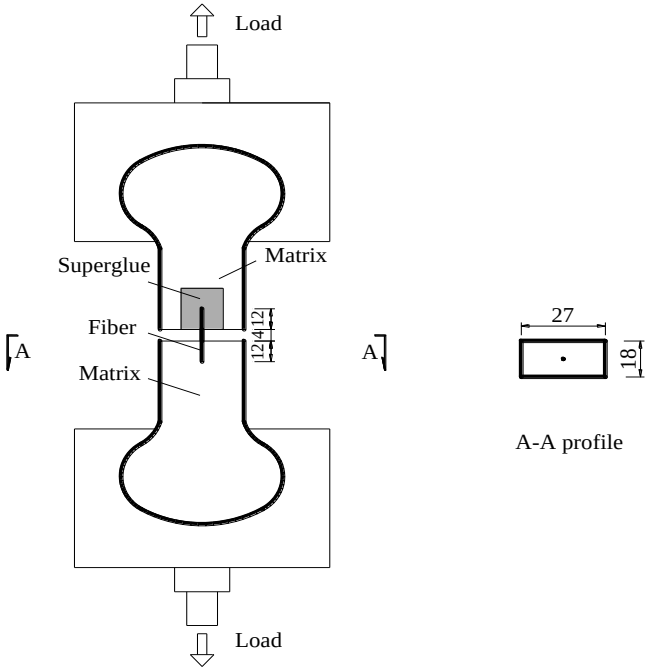


**Fig. 3.** Schematic of the Single Fiber Pull-out Test Set-up (unit: mm).

## Results and Discussion

### Flexural Performance Analysis

The load-deflection curves of different mixtures are represented in Fig. 4. According to the common trends, the load-deflection curves can be divided into three zones, as shown in Fig. 5. In zone 1, the load increased proportionally with the increased deflection up to first cracking. This zone is assumed to be elastic region. In zone 2, damage occurs at the onset of the first cracking and fracture failure initiates within the matrix. The concentrated stress on the crack tip of the matrix is then transferred onto the bridging fiber, leading to the sudden drop after the first cracking in the curves as a result of the lower stiffness of macro-synthetic fibers compared to the matrix. In zone 3, the debonding takes place at the fiber's interface and the fiber can undergo sliding with a slip-hardening effect before the complete failure of FRCs.

According to Fig. 4, all samples display similar curves in zone 1 and zone 2, but not in zone 3. The rapid drop in zone 2 is followed by a second peak, which is much clearer after the addition of mineral admixtures. All mixtures are able to withstand significant post-cracking loads and undergo remarkable deflections, which is due to the fact that the fibers can tightly hold together the two sides of a cracked matrix. Comparison of the flexural responses of each type of concrete clearly shows that the rising process after zone 2 for M0 is much shorter, while other mixtures undergo a continuous growth of post-cracking stress up to the second peak and then lose their load-carrying capacity. The mixtures with the compound incorporation of fly ash and silica fume demonstrate distinct increase in load-carrying capability in zone 3. The remarkable strain-hardening performance, which has metal-like features in tension after the plastic yielding, can be observed in Fig. 4(f) and (g). After the first cracking, the load continues to rise without

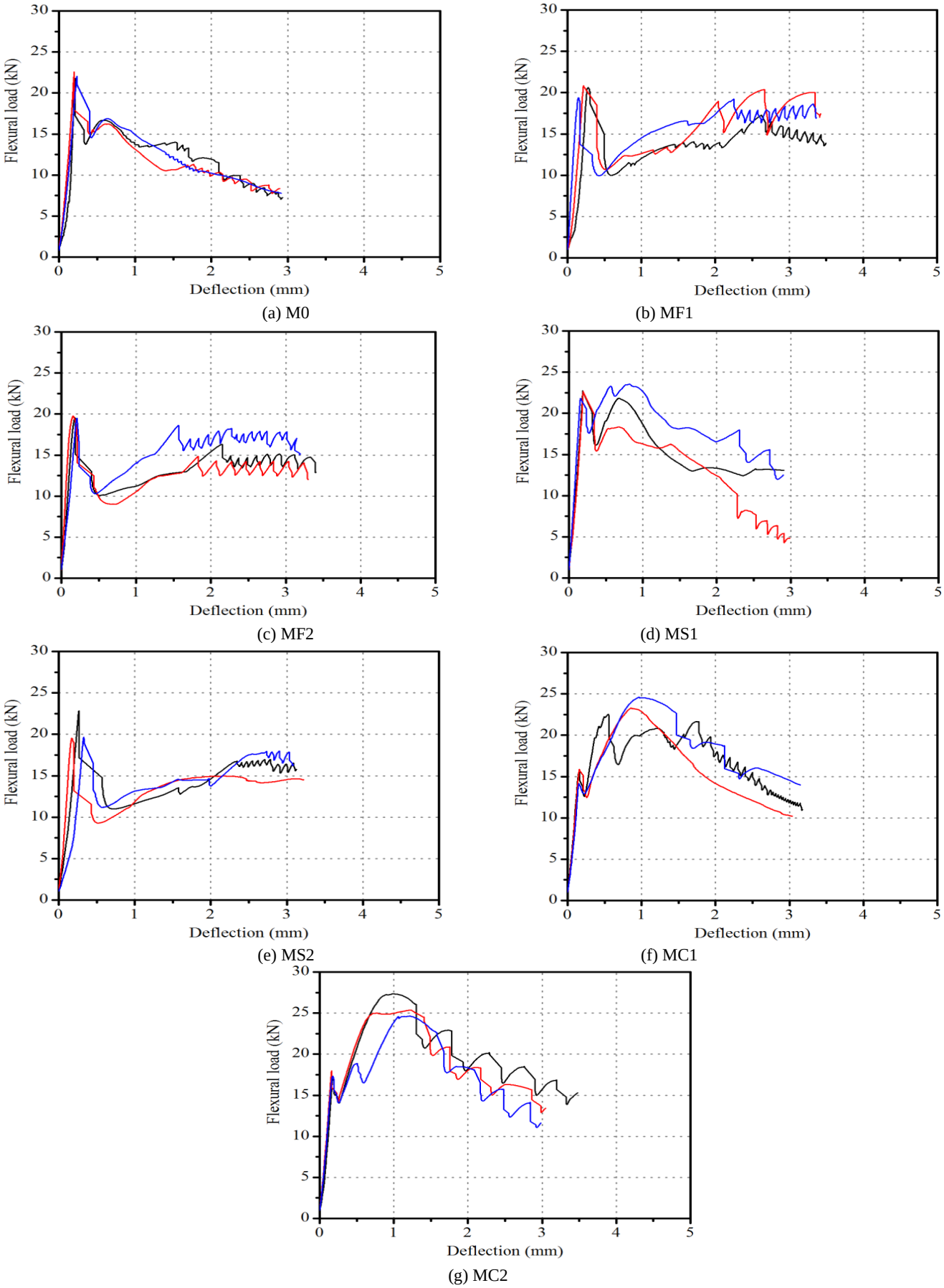


**Fig. 4.** Flexural Load-displacement Curves of All the Mixtures.

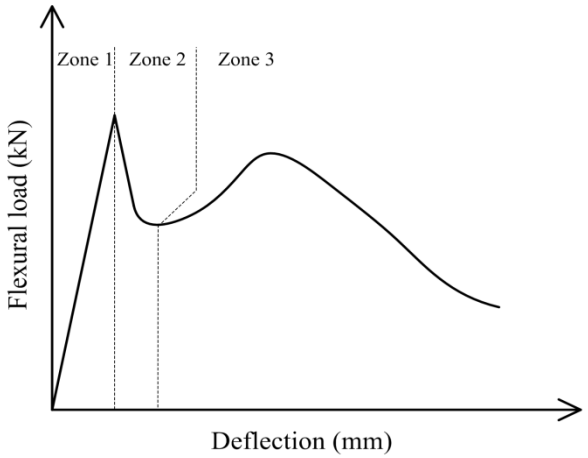


**Fig. 5** Schematic Diagram of Load–deflection Curve.

fracture localization, leading to a greater energy absorption capability.

To facilitate the comparison between the test results of different mixtures, the flexural performances are tabulated in Table 3. The flexural toughness in the present work was determined using the ASTM C1018 test method [15, 16]. According to ASTM C1018, toughness is specified in terms of toughness indices ($I_5$, $I_{10}$ and $I_{20}$), which refers to the area under the load-deflection curve calculated out to three different specified deflections, 3$\delta$, 5.5$\delta$ and 10.5$\delta$ ($\delta$ is the deflection value on the load-deflection curve at first crack).

As shown in Table 3, mixtures that include fly ash show a slight decrease in the ultimate flexural strength compared to M0. And the addition of fly ash causes a slight decrease of $I_5$. However, the toughness indices $I_{10}$ and $I_{20}$ of MF1 and MF2 are higher than those of M0, demonstrating better load-carrying capacity when the strain is high, and better resistance to rapid collapse in zone 3. With the addition of silica fume, a slight increase of ultimate flexural strength is observed. However, the ultimate flexural strength declines when the content of silica fume comes to 10%. The toughness indices of MF1, MF2, MS1 and MS2 are almost at the same level. In the case of mixtures with compound mineral admixtures, there are substantial increases in ultimate flexural strength and mid-span deflection (corresponding to ultimate load) compared to M0. Strain-hardening response appears through cracks propagating, prior to peak load, causing the substantial increase of energy absorption capacity. Therefore, MC1 and MC2 seem to be tougher than the other samples by the larger values of $I_5$, $I_{10}$ and $I_{20}$. It's worth noticing that although the incorporation of compound mineral admixtures leads to different levels of decrease in first crack strength, the ultimate flexural strength for all the mixtures is still much higher than ordinary cement concrete.

## Compressive Strength

The average values of compressive strength for all the concretes are shown in Fig. 6. The cement replacement of mineral admixtures results in noticeable variation for the compressive strength. In general, the compressive strength follows the same trend as does the ultimate flexural strength. Samples with 20% replacement of cement by fly ash (MF2) are proven to have the lowest compressive strength, which could be attributed to the great reduction of hydration products. The detrimental effects of mineral admixtures on strength have sometimes been observed by former researchers [17, 18]. However, it can be concluded that the combination of fly ash and silica fume is a reasonable choice to improve the mechanical properties of FRCs. Besides, the strength values of all the mixtures can fulfill engineering requirements in most projects.

## Interfacial Adhesion Analysis

Pull-out test is a traditional method to evaluate the bond between fiber and cement matrix. The interfacial bonding behaviors of all mixtures in the present work are illustrated by the load-slippage curves in Fig. 7. According to the curves, a significant diversity in their behavior is observed. The addition of fly ash yields a growing decrease in the bond strength, while the mixtures designed with silica fume exhibit moderate improvement in the bonding properties. As expected, the mixtures incorporated fly ash plus silica fume perform better than those prepared with fly ash alone or silica fume alone. This may be attributed to the synergetic effects that leading to the increase of hydration efficiency [19].

On the basis of adhesion theory [2, 20], the fracture energy measured during the separation of fiber and cement matrix is a complex function of the adhesion energy and also of the dissipative parameter:

$$G = W + \varphi \tag{1}$$

where $G$ is practical work of adhesion (energy per unit area of the fracture material), $W$ is the thermodynamic work of adhesion (energy required for breaking of the interfacial chemical interactions) and $\varphi$ is the loss function (energy dissipation during test) which depends on total energy dissipated during fracture. According to the pull-out test results, the value of $G$ can be calculated from

**Table 3.** Flexural Performances of the Mixtures Studied.

| Mix Code | First Crack | | Peak | | Toughness Indices | | |
|---|---|---|---|---|---|---|---|
| | Deflection (mm) | Stress (MPa) | Deflection (mm) | Stress (MPa) | $I_5$ | $I_{10}$ | $I_{20}$ |
| M0 | 0.22 | 6.64 | 0.22 | 6.64 | 4.05 | 7.05 | 12.14 |
| MF1 | 0.22 | 6.09 | 0.22 | 6.09 | 3.82 | 7.88 | 15.02 |
| MF2 | 0.19 | 5.88 | 0.19 | 5.88 | 3.65 | 7.32 | 14.20 |
| MS1 | 0.18 | 6.54 | 0.40 | 6.89 | 4.50 | 8.79 | 16.48 |
| MS2 | 0.26 | 6.21 | 0.26 | 6.21 | 3.83 | 7.93 | 14.37 |
| MC1 | 0.15 | 4.56 | 0.79 | 7.04 | 5.05 | 11.34 | 24.55 |
| MC2 | 0.17 | 5.24 | 1.14 | 7.74 | 5.18 | 11.65 | 24.38 |

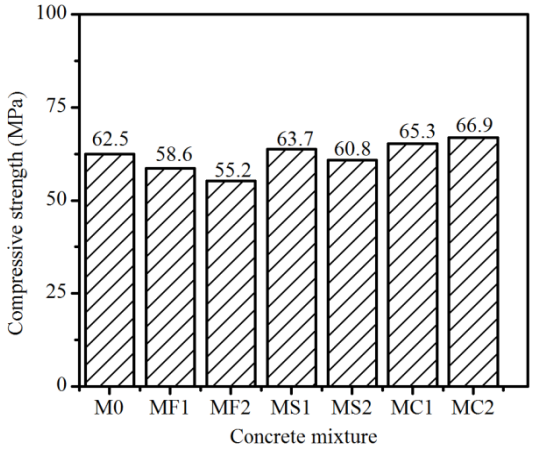


**Fig. 6.** Compressive Strength at 28 Days.

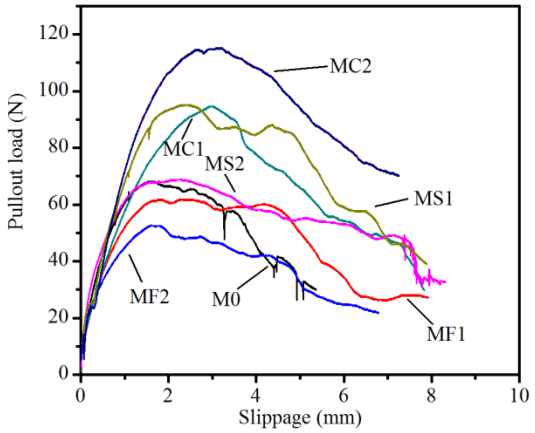


**Fig. 7.** Typical Load-slippage Curves of Single Fiber Pull-out Test

debonding region as following [2]:

$$G = \int_0^{L_d} Fdl / (2\pi d \cdot L) \tag{2}$$

where $F$, $L_d$, $d$, and $L$ are the pull-out load of fibers, the length of the debonded zone, fiber diameter and fiber's length embedded in cement matrix, respectively. The value of $L_d$ was assumed to be the distance between the start and peak point of zone 3.

The results of the pull-out test are calculated and shown in Table 4. Results manifest some interesting features. According to the peak load and corresponding displacement in the pull-out test, the incorporation of mineral admixtures shows different effects on the bonding behaviors depending on the selection of evaluation index. This means that the peak load and corresponding displacement show different trends with the change of proportion. However, the work of adhesion is closely related to the toughness of concrete ($I_{10}$ and $I_{20}$), as shown in Fig. 8. According to Pakravan et al. [7], the work of adhesion is equal to the work done during the pull-out test in the debonding region, which is generated from chemical adhesion and total adhesion energy dissipation, as shown in Eq. (1). This indicates that the higher the work of adhesion, the more energy absorbed during the propagation of cracks. Therefore, the concrete with higher work of adhesion exhibits pronounced enhancement in toughness. So, the work of adhesion is an integrated index to evaluate the bonding between fiber and matrix, which has taken into account both the bonding strength and deformation.

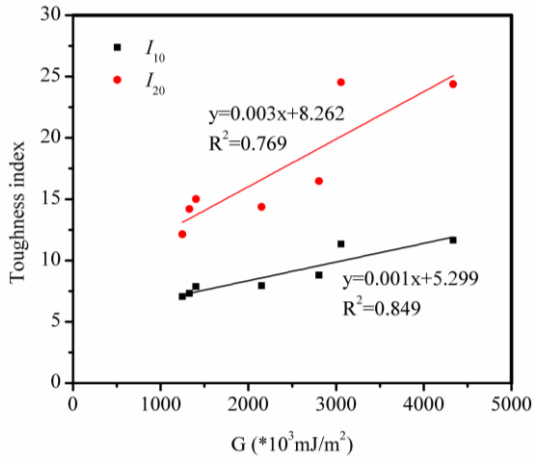


**Fig. 8.** Relationship between Work of Adhesion and Toughness of Concrete

**Table 4.** Average Bonding Properties between Fiber and Matrix for all the Mixtures

| Mix Code | Peak load (N) | Displacement at Peak (mm) | $G$ ($\times 10^3$ mJ/m$^2$) |
|---|---|---|---|
| M0 | 65.39 | 1.51 | 1249 |
| MF1 | 62.28 | 1.68 | 1404 |
| MF2 | 52.96 | 1.76 | 1327 |
| MS1 | 90.67 | 2.38 | 2805 |
| MS2 | 68.50 | 2.49 | 2150 |
| MC1 | 90.49 | 2.46 | 3058 |
| MC2 | 109.35 | 2.81 | 4337 |

## Microstructure Linked Analysis

Fig. 9 shows the microstructure of ITZ between fiber and matrix for M0, MF1, MS1, and MC1. The microstructure observation on the surface shows that a layer of calcium hydroxide (CH) crystals is located at the ITZ, with some needle-like ettringite (AFt) products distributed around it loosely (Fig. 9(a)). This should be attributed to the low chemical affinity between the macro-synthetic fiber, polypropylene fiber in essence, and the hydrophilic cement matrix. Thus, a relatively large gap filled by water can develop between the fiber and matrix. And this hollow space is a sustainable situation for growing CH crystals as a result of the greater mobility of calcium ions in a water environment [11]. Due to the brittle feature of CH crystals [17] and low density of ITZ, the fiber in M0 samples is prone to debond and pull-out.

In the case of MF1, most of the CH gathered in the ITZ is consumed by the pozzolanic reaction of fly ash to form C-S-H gel. Although the increased amount of C-S-H gel occupies the voids in ITZ and enhances the bond between the inclusion and the bulk matrix, the pores still exists, as shown in Fig. 9(b). Previous research has reported that different types of cement hydrates in the ITZ had different tendencies in influencing the principle that the stress is transferred from the bulk matrix to the fiber [17, 21]. The ductile bond formed between C-S-H and macro-synthetic fiber's

interface is beneficial for the slippage of fiber in the matrix before failure of bonding. Therefore, the work of adhesion for the fiber of MF1 is improved mildly, leading to the better load-carrying capacity when the strain is high and resistance to rapid collapse. The continued addition of fly ash in MF2 might decrease the amount of hydration products as the replacement of fly ash, retarding the growth of strength. This explains the slight drop of flexural strength and pull-out load in Table 3 and Table 4, respectively. Accordingly, the incorporation of fly ash only may be detrimental to achieving desired mechanical properties.

The addition of silica fume accelerates the transformation of CH crystals into C-S-H gel due to its high content of amorphous silica ($SiO_2$) (85% in general). Thus, no CH was found during the microstructure observation, as shown in Fig. 9(c). According to Ba and Bosiljkov [18, 22], the filler function of silica fume acts as a nucleation site and accelerates the hydration of clinker minerals. Therefore, the silica fume particles permeate into the small spaces between fiber and matrix with the diffusion of water solution during the ‘‘bleeding” process due to its smaller particle size and microsphere morphology, as shown in Fig. 1(b). Then, the particles form nucleation sites and accelerate the hydration, resulting in an improvement in the strength. As for MS2 with a larger percentage of silica fume (10%), the strength declines rather than grows. Excessive addition of silica fume can considerably impair the fluidity of the fresh mixture as a result of the high specific surface area of silica fume, leading to the poor dispersion of silica fume in the matrix and decrease of strength. This finding fits well with that of Lee and Yogendran [17, 23].

As exhibited in Fig. 9(d), the microstructure of the ITZ with the compound addition of fly ash and silica fume is more uniform and compact than that of the former mixtures. The clusters of C-S-H grow outward and interweave with each other, forming a more close-connected hydration structure. This can be attributed to the grading hydration and filling effect of the compound system [19]. The improvement of hydration packing of the ITZ is expected to develop a more compact and stronger bond between the fiber and matrix. Therefore, MC1 and MC2 demonstrate much better properties in flexural strength and fracture resistance.

The effects of mineral admixtures on micro-hardness of the ITZ are shown in Fig. 10. The distance studied from the fiber’s interface in the micro-hardness test is from 5 up to 70 μm. In order to guarantee the test point within a specified distance, parallel lines were made using the tip of the indenter under different levels of distance. Each data point in each curve shown in Fig. 10 represents an average value of three points at the same distance. It shows that micro-hardness increases gradually with the increasing distance away from the fiber and then it reaches a plateau at 40 to 60 μm. With the addition of admixtures, the ITZ between fiber and matrix is greatly enhanced. And the adoption of compound admixtures has better effect. The micro-hardness of MC2 almost comes to a constant value at 40 μm away while the distance of M0 is about 60 μm. Although the total dosage of admixtures in MC1 is smaller than MF2, the micro-hardness of MC1 is still much higher than all the samples with single admixture.

It’s reported that the influence factor of micro-hardness includes the compact degree and hydration products around the ITZ [24].

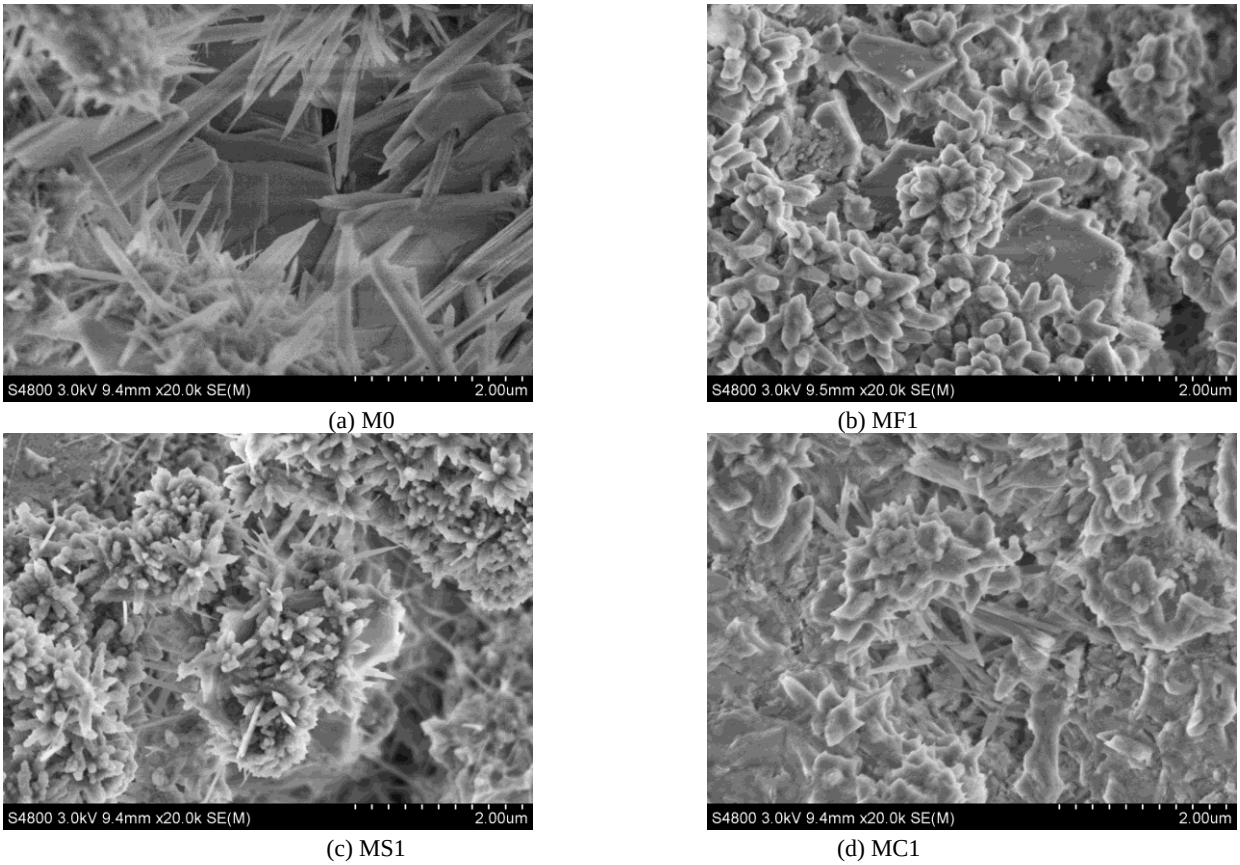


(a) M0 (b) MF1

(c) MS1 (d) MC1

**Fig. 9.** SEMs of ITZ between Fiber and Matrix.

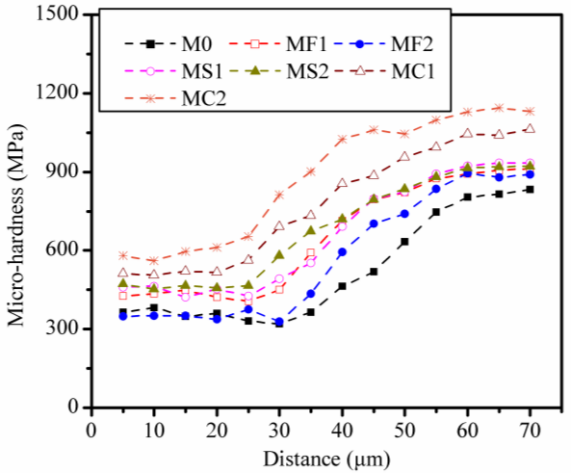


**Fig. 10.** Effects of Mineral Admixtures on Micro-hardness of the ITZ.

The improvement of compact degree and amount of C-S-H increases the resistance during the fiber slippage. Therefore, the synergistic effect of micro-aggregate filling and pozzolanic reaction of fly ash and silica fume optimizes the microstructure of concrete, enhancing the bonding behavior between macro-synthetic fiber and matrix, thereby leading to the substantial increase of toughness as discussed above. Accordingly, it can be concluded that the adoption of fly ash plus silica fume can optimize the particle size distribution and enhance the rate of cement hydration in FRCs.

## Conclusions

(1) All concrete mixtures prepared with macro-synthetic fiber are able to withstand significant post-cracking loads and undergo significant deflections under flexural loads due to the bridging effect of macro-synthetic fiber which can tightly hold together the two sides of a cracked matrix. The maximum flexural and compressive strength are noted in MC2 specimens, while the minimum are noted in MF2 specimens. The flexural toughness of concrete incorporating fly ash plus silica fume is much better than those prepared with either fly ash or silica fume alone.

(2) The work of adhesion is an integrated index to evaluating the bonding behaviors between fiber and matrix. The results of work of adhesion exhibit a trend similar to that noted in the flexural toughness. The maximum work of adhesion is noted in MC2 specimens, while the minimum is noted in M0 specimens. The synergistic effect of micro-aggregate filling and pozzolanic reaction of fly ash plus silica fume provides a marginal improvement in the work of adhesion.

(3) The mineral admixtures improve the microstructure of the ITZ. Compound incorporation of fly ash + silica fume presents the most distinct improvement effects, then the silica fume. FRC with higher micro-hardness and denser micro-morphology has correspondingly higher strength and fracture resistance. C-S-H amount and compaction of ITZ play key roles in the fiber - matrix interfacial bond and the mechanical properties of concrete. Compound incorporation of mineral admixtures is a reasonable method to achieve the desired mechanical properties of macro-synthetic fiber reinforced concrete.

## Acknowledgements

The findings in this paper are supported by the Research Fund for the Doctoral Program of Higher Education of China (Grant No. 20130205110013), the Nature Science Foundation of China (Grant Nos. 51208047 and 51308062), China Postdoctoral Science Foundation (Grant No. 2014M552397), Natural Science Foundation of Shaanxi Province (2014JM7272), and Key Laboratory of Road and Traffic Engineering of the Ministry of Education, Tongji University (K201402).

## References

1. Hsie, M., Chen, G., and Song, P. (2011). Investigating Abrasion Resistance of Steel-polypropylene Hybrid Fiber-reinforced Concrete Using Statistical Experimental Design. *International Journal of Pavement Research and Technology*, 4(5), pp. 274-280.
2. Pakravan, H.R., Jamshidi, M., Latifi, M., and Chehimi, M.M. (2012). Polymeric Fibre Adhesion to the Cementitious Matrix Related to the Fibres Type, Water to Cement Ratio and Curing Time. *International Journal of Adhesion & Adhesives*, 35, pp. 102-107.
3. He, R., Chen, S.F., Li, Y.P., Cong, P.L., and Liu, Z.Z. (2012). Chemical Resistance of Polyvinylalcohol Reinforcing Fibers, *International Journal of Pavement Research and Technology*, 5(4), pp. 277-282.
4. Zhang, Z.H., Yao, X., Zhu, H.J., Hua, S.D., and Chen, Y. (2009). Preparation and Mechanical Properties of Polypropylene Fiber Reinforced Calcined Kaolin-fly Ash Based Geopolymer. *Journal of Central South University*, 16, pp. 49-52 (in Chinese).
5. Caggiano, A., and Martinelli, E. (2012). A Unified Formulation for Simulating the Bond Behaviour of Fibres in Cementitious Materials. *Materials and Design*, 42, pp. 204-213.
6. Laranjeira, F., Molins, C., and Aguado, A. (2010). Predicting the Pullout Response of Inclined Hooked Steel Fiber. *Cement and Concrete Research*, 40(10), pp. 1471-1487.
7. Pakravan, H.R., Jamshidi, M., Latifi, M., and Pacheco, F. (2012). Evaluation of Adhesion in Polymeric Fibre Reinforced Cementitious Composites. *International Journal of Adhesion & Adhesives*, 32, pp. 53-60.
8. Tosun, K., and Felekoglu, B. (2013). Effects of Fiber-matrix Interaction on Multiple Cracking Performance of Polymeric Fiber Reinforced Cementitious Composites. *Composites: Part B*, 52, pp. 62-71.
9. Sun, W., and Yan, Y. (1994). Study of the Interfacial Effect and Fatigue Behaviour of Steel Fiber Reinforced High Strength Cement Based Composite Materials. *Journal of the Chinese Ceramic Society*, 22(2), pp. 107-116 (in Chinese).
10. Hu, L.Q., Wu, S.P., Nan, C.W., and Hu, S.G. (2001). The Interfacial Characteristic of Steel Fiber Reinforced Polymer Cement Composite. *Journal of Wuhan University of*

*Technology*, 23(12), pp. 20-23 (in Chinese).

11. Sadrmomtazi, A., and Fasihi, A. (2010). Influence of Polypropylene Fibers on the Performance of Nano-$SiO_2$-incorporated Mortar. *Iranian Journal of Science & Technology, Transaction B: Engineering*, 34(B4), pp. 385-395.
12. Buratti, N., Mazzotti, C., and Savoia, M. (2011). Post-cracking Behaviour of Steel and Macro-synthetic Fibre-reinforced Concretes. *Construction and Building Materials*, 25(5): 2713-2722.
13. Erdem, S., Dawson, A.R., and Thom, N.H. (2011). Microstructure-linked Strength Properties and Impact Response of Conventional and Recycled Concrete Reinforced with Steel and Synthetic Macro Fibres. *Construction and Building Materials*, 25(10), pp. 4025-4036.
14. Xing, M.L., He, R., Chen, S.F., and Li, Y.P. (2013). Mechanical Properties and Impermeability of High Performance Cementitious Composite Reinforced with Polyethylene Fibers. *International Journal of Pavement Research and Technology*, 6(3), pp. 239-242.
15. ASTM C1018-97 (1997). Standard Test Method for Flexural Toughness and First-crack Strength of Fiber-reinforced Concrete, ASTM International, West Conshohocken, PA, USA.
16. Sukontasukku, P. (2004). Toughness Evaluation of Steel and Polypropylene Fibre Reinforced Concrete Beams Under Bending. *Thammasat International Journal of Science and Technology*, 9(3), pp. 35-41.
17. Lee, S.F., and Jacobsen, S. (2011). Study of Interfacial Microstructure, Fracture Energy, Compressive Energy and Debonding Load of Steel Fiber-reinforced Mortar. *Materials and Structures*, 44(8), pp. 1451-1465.
18. Ba, H.J., Feng, Q., and Yang, Y.Z. (2002). Hydration Reaction Between $C_3S$ and Fly Ash, Silica Fume, Nano-$SiO_2$ and Microstructure of Hydrated Pastes. *Journal of the Chinese Ceramic Society*, 30(6), pp. 780-784 (in Chinese).
19. Luo, Z.T. (2010). *Hydration Mechanism and Synergistic Effect of the Cement-based CaO and $SiO_2$-$Al_2O_3$ Composite Materials*, PhD Dissertation. Wuhan University of Technology, Wuhan, China (in Chinese).
20. Peled, A., Zaguri, E., and Marom, G. (2008). Bonding Characteristics of Multifilament Polymer Yarns and Cement Matrices. *Composites: Part A*, 39, pp. 930-939.
21. Tabor, D. (1981). Principles of Adhesion-bonding in Cement and Concrete, in: Peter C Kreijger (Ed.), *Adhesion Problems in the Recycling of Concrete, N.A.T.O. Conference Materials Science*, Plenum Press, New York, USA, pp. 63-87.
22. Bonavetti, V., Donza, H., Rahhal, V., and Irassar, E. (2000). Influence of Initial Curing on the Properties of Concrete Containing Limestone Blended Cement. *Cement and Concrete Research*, 30(5), pp. 703-708.
23. Yogendran, V., Langan, B.W., Haque, M.N., and Ward, M.A. (1987). Silica Fume in High-strength Concrete. *ACI Materials Journal*, 84(2), pp. 124-129.
24. Duan, P., Shui, Z.H., Chen, W., and Shen, C.H. (2013). Efficiency of Mineral Admixtures in Concrete: Microstructure, Compressive Strength and Stability of Hydrate Phases. *Applied Clay Science*, 83-84, pp. 115-121.